SUPPORTING INFORMATION

Cameroonian Natural Clay Derived Linde type LTA Zeolite: Demystifying and Understanding the Impact of the Synthesis Process on Adsorption Efficiency

Cyrille Ghislain Fotsop[a], Alexandra Lieb[a], Franziska Scheffler[a]

[a] Otto-von-Guericke-University Magdeburg, Chemical Institute, Chair for Industrial Chemistry, Universitätsplatz 2, 39106, Magdeburg, Germany

Tab. S1. XRF analysis of zeolite NaA (Z-MK-900 and Z-AF-900)

Sample	**Zeolite NaA**	
Molar (%)	**Z-MK-900**	**Z-AF-900**
SiO_2	26.27	24.83
Al_2O_3	24.57	22.18
Na_2O	16.00	18.76
K_2O	0.04	0.02
MgO	0.001	0.001
CaO	0.03	0.02
TiO_2	0.65	0.70
MnO	0.00	0.00
$F_{e2}O_3$	0.31	0.30
H_2O	12.00	13.00
ZnO	0.00	0.00
ZrO_2	0.005	0.005
LOI	20.00	20.00
Total	99.89	99.94

Tab. S2. Physicochemical properties of Z-AF-S1 and Z-MK-S1 samples

Samples	BET surface area ($m^2.g^{-1}$)	Micropore volume ($cm^3.g^{-1}$)	Total pore volume ($cm^3.g^{-1}$)
Z-AF-S1	32.3	0.0207	0.078
Z-MK-S1	50.8	0.0120	0.043

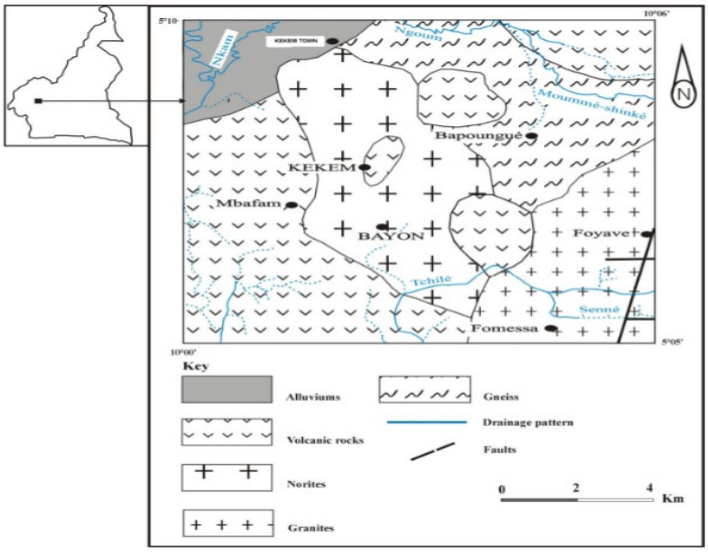

Fig. S1. Geological map and location of the Kekem City

1. Optimization of factors during the synthesis of zeolites NaA

Different factors affecting the formation of zeolites NaA, including dosage of aluminum mass, sodium hydroxide concentration, time and temperature of crystallization were investigated in relation to obtained metakaolin by AF method.

1.1. The impact of aluminum mass

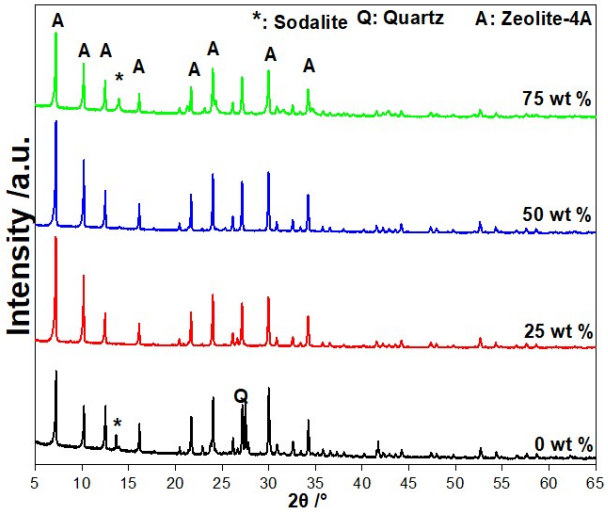

Fig. S2. XRD pattern of influence of aluminum mass during the synthesis of zeolite NaA using metakaolin achieved by AF method

1.2. Effect of crystallization temperature

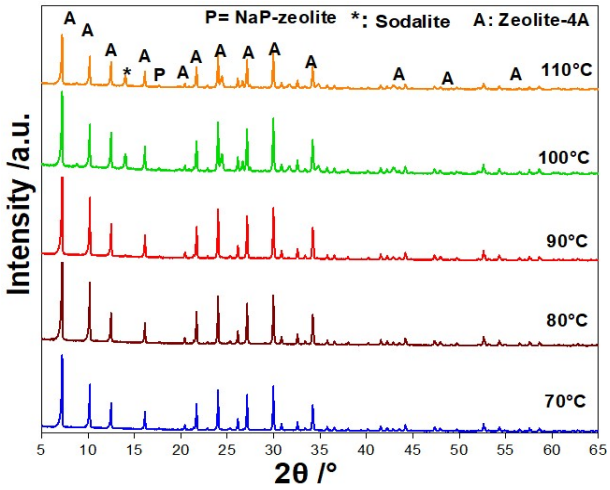

Fig. S3. XRD pattern of synthesized samples using different temperatures of crystallization

1.3. Effect of crystallization time

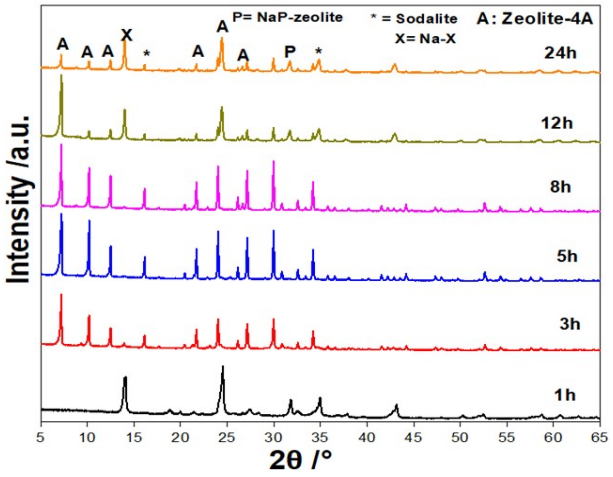

Fig. S4. XRD pattern of synthesized samples using different crystallization time

1.4. Effect of concentration

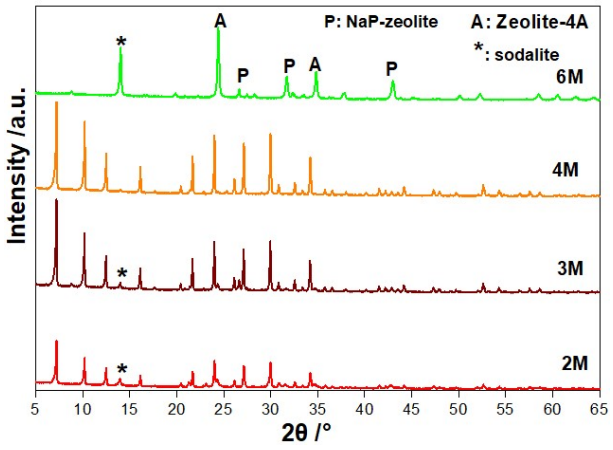

Fig. S5. XRD pattern of synthesized samples using different concentration of sodium hydroxide

1.5. CO_2 adsorption isotherm

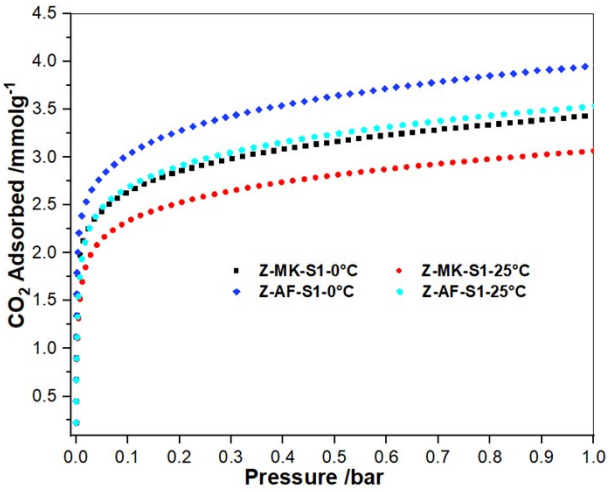

Fig. S6. CO_2 adsoption capacity on zeolite Z-AF-S1 and Z-MK-S1 at 0°C and 25°C

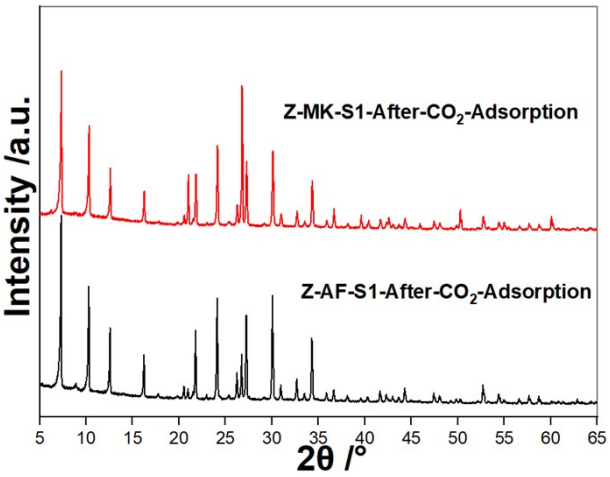

Fig. S7. XRD pattern of Z-MK-S1 and Z-AF-S1 after CO_2 adsorption-desorption

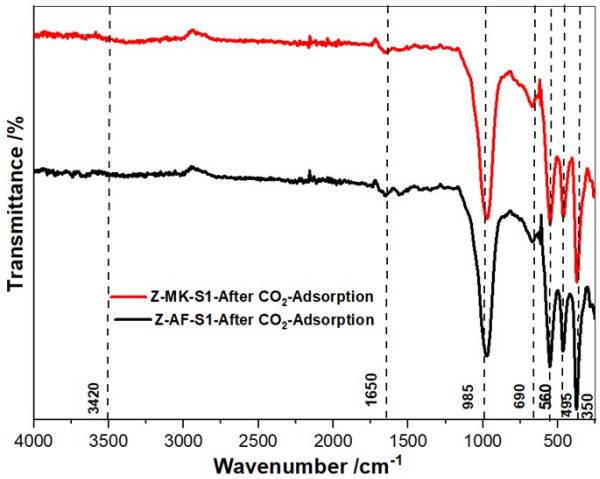

Fig. S8. FTIR spectra of Z-MK-S1 and Z-AF-S1 after CO_2 adsorption-desorption

2. Isotherm modeling

Tab. S3. Langmuir, Freundlich, Dual site Langmuir (DSL), Dual site Langmuir-Freundlich (DSLF) and Dual site Langmuir Sips (DSLSips) parameters for CO_2 adsorption on Z-AF-S1 and Z-MK-S1 at relative pressure and equilibrium temperature

Isotherm	Parameters	Z-AF-S1/Temperature (°C)		Z-MK-S1/ Temperature (°C)	
		0	25	0	25
Langmuir	q_{max}	52.417	38.214	435.776	126.461
	k	3.814	3.452	3.104	2.834
	R^2	0.7518	0.8651	0.87645	0.9213
Freundlich	k_f	4.043	3.645	3.511	3.156
	t	6.88	6.072	6.968	6.157
	R^2	0.965	0.956	0.9607	0.9544
DSL	q_{max1}	1.793	2.317	2.185	1.339
	k_1	4.179	441.045	1510.683	3.001
	q_{max2}	2.461	1.554	1.523	2.037
	k_2	1684.35	3.213	3.936	408.205
	R^2	0.9982	0.9983	0.9987	0.9985
DSLF	q_{s1}	1.794	2.317	2.185	2.037
	k_1	0.008	8.837	3.479	3.672
	t_1	0.002	0.020	0.003	0.009
	q_{s2}	2.461	1.554	1.523	1.339
	k_2	2.737	4.093×10^{-7}	0.024	8.216×10^{-5}
	t_2	0.0016	1.273×10^{-7}	0.006	2.737×10^{-5}
	R^2	0.9982	0.9983	0.9988	0.9986
DSLSips	q_{max}	2.217	1.826	1.948	1.585
	k_1	1894.264	8.329	1698.365	8.288
	k_2	1.420	984.684	1.199	1174.915
	t	0.490	1.152	0.465	1.373
	R^2	0.9993	0.9931	0.9997	0.9926

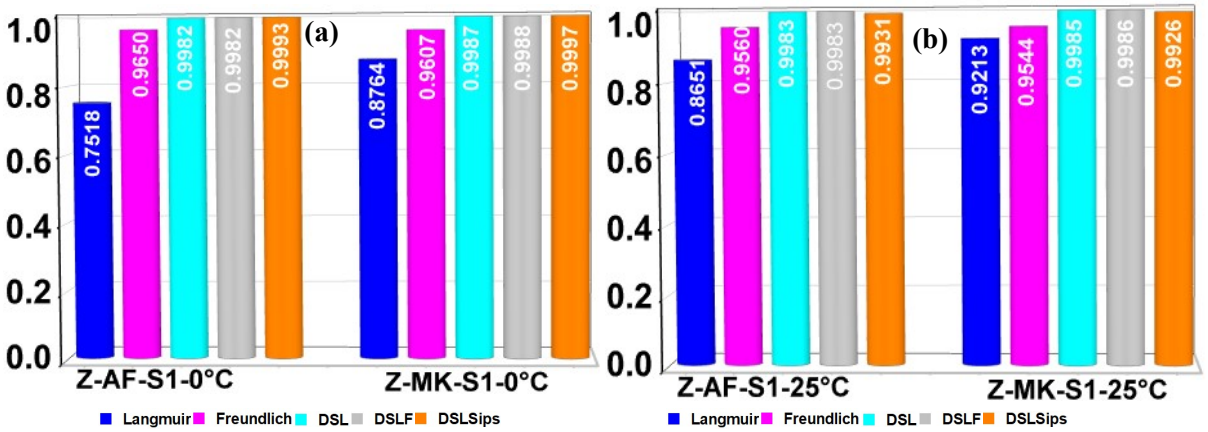

Fig. S9. Coefficients of correlation (R^2) of fitted model isotherm at 0°C (a) and 25°C (b) for Z-AF-S1 and Z-MK-S1. The blue, magenta, cyan, gray and orange cones denote the Langmuir, Freundlich, Dual site Langmuir (DSL), Dual site Langmuir-Freundlich (DSLF) and Dual site Langmuir Sips (DSLSips) isotherm models respectively

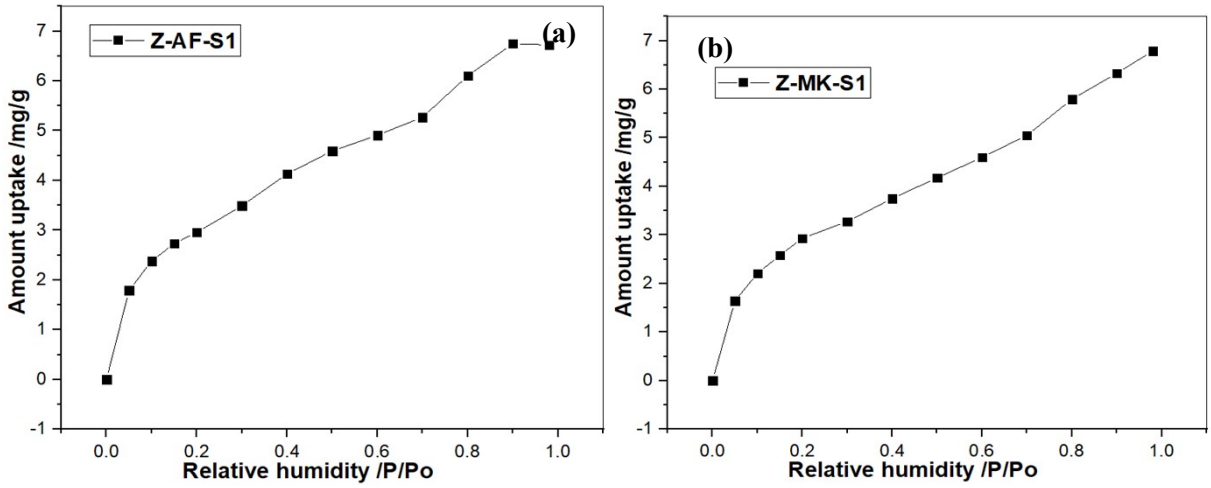

Fig. S10. Experimental water vapor adsorption isotherms for Z-AF-S1 (a) and Z-MK-S1 (b) at 20 °C